Pavement rutting performance analysis of automated vehicles: impacts of wander mode, lane width, and market penetration rate

Journal Name: International Journal of Pavement Engineering

Pavement rutting performance analysis of automated vehicles: impacts of wander mode, lane width, and market penetration rate

Ali Yeganeh[a*], Bram Vandoren[a], Ali Pirdavani[a, b]

[a]*UHasselt, Faculty of Engineering Technology, Agoralaan, 3590 Diepenbeek, Belgium*

[b]*UHasselt, The Transportation Research Institute (IMOB), Agoralaan, 3590 Diepenbeek, Belgium*

Corresponding author; Tel: +32494652590; *E-mail address:* ali.yeganeh@uhasselt.be

Word count: 10559 words

Abstract

The programmable capability of automated driving technologies in recent years would allow the design of different lateral wandering patterns for automated vehicles (AVs). One of the significant contributing factors in wheel-wander design is the lane width. The AVs' deployment with the gradual market penetration rate increase and different wander modes combined with the lane width effect would lead to different load distribution scenarios, impacting the pavement performance. This study compares pavement rutting damages induced by different load distribution scenarios resulting from the coexistence of AVs and human-driven vehicles (HDVs). To this end, the present study assumed several load distribution scenarios by setting out different penetration rates (i.e., 0%, 20%, 40%, 60%, 80%, and 100%), wander modes (i.e., zero-, normal-, uniform-time-, and uniform-frequency-wander), and different lane width scenarios (i.e., 3 m, 3.25 m, and 3.5 m). A finite element model of a full-depth flexible pavement was developed using ABAQUS software to evaluate the pavement rutting damage. The results showed that the significance level of differences between rutting damages induced by different wander modes and different lane width scenarios is substantially influenced by the AVs' penetration rate. For instance, in the higher penetration rates, the differences between the rutting performance of different wander modes are more significant than in the lower penetration rates. Furthermore, the lane width effect becomes more significant in the segregated scenario with 100% AVs than in the integrated scenarios in normal- and uniform-wander modes. Accordingly, AVs' penetration rate is a decisive factor in the practical decision-making process in the wander mode determination and lane width design for AVs.

Keywords: automated vehicle; pavement rutting performance; penetration rates: wander effect; finite element model; lane width effect

Introduction

Automated vehicles' deployment may affect the roads' pavement performance and cause a drastic change in pavement analysis and design (Chen, Balieu and Kringos, 2016; Noorvand and Underwood, 2017; Chen et al., 2019; Zhou et al., 2019; Chen, Song and Ma, 2020; Gungor and Al-Qadi, 2020a, 2020b; Rana and Hossain, 2021; Yeganeh, Vandoren and Pirdavani, 2021). One of the most significant aspects of AVs', which might influence pavement loading, is the AVs' different possible lateral wandering patterns. In 2016, Chen et al. (2016) brought up the idea that AVs' automatic lateral control system could reduce the wheel-wander range. The results of their finite element simulations showed that a reduced wheel-wander might have the potential to accelerate the pavement rutting damage significantly. In 2017, Noorvand and Underwood (2017) introduced zero- and uniform-wander distributions as two potential wander modes for AVs. They devised a methodology to account for these wander modes within the variables available in the Mechanistic-Empirical Pavement Design Guide (MEPDG) (McCullah and Gray, 2005). They showed that the uniform-wander mode could increase pavement life because it would allow the vehicles to use a wide range of lane space. However, the authors' previous study (Yeganeh et al., 2021) argued that the AVs' implication in a dedicated lane with both zero-wander and the uniform-time-wander mode would cause abrupt changes in the edges of the loading schemes and would accelerate the pavement damage in the edges of the loading area when compared to the human-driven vehicles' (HDVs') lane. In addition to zero- and uniform-wander distributions, Chen et al. (2019) proposed two other possible lateral wandering modes for AVs, named double peak Gaussian and two-section uniform modes. Their study's finite element simulation results showed that using peak Gaussian and two-section uniform modes can increase the pavement life. In another study, Song et al. (2021) conducted a study to investigate the truck platooning effect on pavement damage, considering the fuel consumption. Using computational fluid dynamic (CFD) simulation

and finite element analysis, they compared the fuel-saving and fatigue damage caused by two-truck platoon with and without a lateral offset between trucks. Their results showed that considering the lateral offset of 50 mm, 100 mm, and 150 mm in a two-truck platoon would decrease the pavement fatigue damage by 8.5%, 30.45%, and 41.2%, respectively, compared with the no-lateral offset condition.

In addition to AVs' lateral wandering pattern effects, the other crucial aspect of AVs' deployment that can influence the pavement performance is the lane distribution for the combination of AVs and HDVs on the roads. AVs may use shared travel lanes (i.e., integrated scenarios) at different penetration rates, or it is possible to use dedicated lanes (i.e., segregated scenarios) only for AVs. In recent years, there has been an increasing amount of literature on studying the effects of using different lane distribution policies for the interactions between AVs and HDVs on different aspects of the transportation system operation and design (Liu and Song, 2019; Mohajerpoor and Ramezani, 2019; Amirgholy, Shahabi and Oliver Gao, 2020; Razmi Rad et al., 2020). However, little attention has been drawn to the effects of lane distribution of AVs and HDVs on pavement performance (Noorvand and Underwood, 2017; Chen et al., 2019; Rana and Hossain, 2021). In this regard, Noorvand and Underwood (2017) investigated the design thickness and initial construction costs for both segregated and integrated scenarios. They showed the advantages of the segregated scenario over the integrated scenario in several cases for combinations of automated and non-automated trucks. In another study, Chen et al. (2019) investigated the effects of different proportions of HDVs in a lane and confirmed its significant effects on pavement life. They showed that by increasing the percentage of AVs with zero-wander mode from 0% to 100%, the pavement's rutting depth increases, and the maintenance year is advanced by a maximum of 1.56 years. Conversely, the rutting performance was improved using

the uniform-wander, double peak Gaussian, and two-section uniform modes for AVs compared with the rutting induced by HDVs. They demonstrated that when the AVs' penetration rate is more than 50%, applying the two-section uniform-wander mode for AVs delays the maintenance year by 2.3 years. Rana and Hossain (2021) simulated the autonomous trucks' pavement performance through the Mechanistic-Empirical Pavement Design Software, AASHTOWare, to minimize the pavement distresses by controlling the wander distribution and lane sharing scenarios. They simulated both separated and integrated scenarios, and they classified the integrated scenarios into equally distributed and disproportionately distributed cases. Their findings showed that the equally distributed autonomous trucks could significantly decrease the pavement damage.

Moreover, the AVs' deployment can also influence the lane width design for AVs and HDVs. In other words, the automatic lateral wandering control of AVs may imply a narrower lane width to save construction and maintenance costs. Consequently, this reduced lane and lateral wandering distance can affect pavement performance. However, to the best of our knowledge, no previous study has investigated the impacts of lane width together with lateral wandering and penetration rates on pavement performance. Therefore, this paper will investigate the impacts of AVs' penetration rates on pavement rutting performance combined with lane width and wander distributions' effects and consider both segregated and integrated scenarios. In addition to the zero-wander mode, this study presents two different potential formulations for the implication of the uniform-wander mode, namely uniform-time and uniform-frequency, to give a better practical insight into the application of uniform-wander mode for AVs. Furthermore, this paper introduces and studies the potential normal-wander mode for AVs with theoretical standard deviations and compares it with the normal-wander distribution for HDVs with empirical standard deviations for different lane widths.

Methodology

This study considers potential combinations of HDVs and AVs with different AVs' penetration rates and wander modes in different lane widths to simulate the in-service pavement rutting performance. For this purpose, this study used a finite element model validated based on the Indiana Department of Transportation/Purdue University accelerated pavement tester (APT) facility. Since the pavement design depends primarily on truck traffic, only trucks are considered in our analysis, and the acronym AVs only denotes the automated trucks in this paper. The following sections describe the evaluation scenarios, finite element modelling and validation, in-service rutting performance simulation, and wheel-wander calculation.

Evaluation scenarios

To date, there has been little agreement on how AVs and HDVs will interact in the future. One of the most significant current discussions is on the consequences of using either the same travel lanes (i.e., integrated scenario) or separate lanes (i.e., segregated scenario) for AVs (Liu & Song, 2019; Mohajerpoor & Ramezani, 2019; Razmi Rad et al., 2020). This study evaluates both segregated and integrated scenarios, considering the AVs' different penetration rates effects on a flexible pavement system from the pavement rutting performance perspective. Accordingly, this study set the AVs' penetration rates to be 0% (i.e., a segregated scenario with only HDVs), 20%, 40%, 60%, 80%, and 100% (i.e., a segregated scenario with only AVs).

Since the lateral wandering patterns for AVs can be different from HDVs and have significant effects on the pavement rutting performance, this study considers three possible lateral wandering patterns for AVs, naming "zero-wander", "normal-wander", and "uniform-wander" patterns. The uniform-wander mode is formulated in two different approaches, namely, "uniform-time" and "uniform-frequency". The present study, considered a normal distribution for the HDVs' lateral

wandering pattern, which is confirmed by previous studies (Buiter et al., 1989; Erlingsson, 2004; Timm and Priest, 2005; Siddharthan et al., 2017). These studies generally concluded that the normal-wander distributions' standard deviation could be affected by the traffic lane's width. This study examined lane widths of 3 m, 3.25 m, and 3.5 m. It is worth mentioning that this study assumes that AVs could comply with the same speed limit and narrower lanes accommodating similar traffic volumes. In this regard, one of the promises of AVs is their advanced braking system, which could decrease the braking distance and consequently decrease the distance between the vehicles. In addition to this, the sensing reaction time (SRT) for AVs could be lower than HDVs (Binshuang et al., 2019). This could also reduce the traffic headways resulted in shorter gaps between vehicles. Thus, the reduced stopping distance for AVs, along with the automated steering control of them could promise to preserve traffic safety in narrower lanes in addition to an increase in road capacity. Furthermore, since the focus of this study is the impact of lane width on wander distributions and consequently on pavement rutting performance, all factors are kept the same, except the lane width and wander mode.

In total, this study considered three main scenarios as follows:

- Reference scenario: in this scenario, the AVs' penetration rate is 0%, and only HDVs use the road. The lane width is assumed to be 3 m, 3.25 m, and 3.5 m. This scenario was used as reference cases to evaluate the other scenarios.
- Integrated scenario: this scenario represents a mixed traffic condition and is more likely to exist in the near future. In this scenario, AVs with different penetration rates of 20%, 40%, 60%, 80%, and wander distribution of zero, normal, uniform-time, or uniform-frequency will use a shared lane with HDVs with normal distribution. The lane widths of 3 m, 3.25 m, and 3.5 m were considered for each case.

- Segregated scenario: in this scenario, the AVs' penetration rate is 100%, representing a dedicated lane for AVs. Wander distributions and lane widths were assumed similar to scenario 2.

Finite element modelling and validation

The present study used the FE modelling approach, which has been confirmed as a powerful method with the capability of modelling pavement rutting performance (Huang, 1995; Hua, 1998; Hua and White, 2002; White et al., 2002; Ali, Sadek and Shahrour, 2008; Saevarsdottir and Erlingsson, 2015). The present work utilized the commercial software ABAQUS (Smith, 2009) to conduct the required simulations. To develop a FE model, this study used the characteristics of the Indiana Department of Transportation/Purdue University accelerated pavement tester (APT) facility, which has been utilized in several studies on hot mix asphalt (HMA) rutting performance (Huang, 1995; Hua, 1998; Hua and White, 2002). Since the FE model should be calibrated and validated to be used in this study, all the model geometry, material properties, and modelling conditions were selected based on Hua et al.'s (1998) study. Accordingly, the APT facility's pavement structure includes a 0.076 m asphalt overlay on top of a reinforced concrete slab and pea gravel, which acts as a rigid foundation. A length of 1.27 m was selected for the 3D FE model in this study (Hua, 1998). The bottom boundary condition is assumed fixed. The boundary nodes along the pavement edges are horizontally constrained but are free to move in the vertical direction.

Material model

Rutting is defined as the permanent deformation of flexible pavement accumulated by increasing the number of load repetitions. To simulate the rutting performance mechanically, the material model should have the capability to calculate the strain responses of the pavement

subjected to the vehicular load and predict the strain accumulations under variable loading times and temperatures. From the martial model point of view, the application of vehicular load on the surface of the asphalt layer could cause three different types of strains: (1) elastic recoverable, (2) viscoelastic, and (3) irrecoverable plastic strains (Perl, Uzan, and Sides 1983).

According to the viscoelastic theory, the isotropic viscoelastic behaviour of asphalt mixture can be characterised by elements such as the Hookean spring and the Newton dashpot. For instance, the generalised Kelvin-Voigt (1892) solid model (i.e., a spring and a number of Voigt elements connected in series), a generalised Maxwell (1867) solid model (i.e., a spring and a number of Maxwell elements connected in parallel) may be used. However, the original forms of these models could not consider creep or plastic strain. Later, the combination of the Maxwell model and the Kelvin model was proposed (i.e., Burgers' model (1935)), predicting the short-term viscoelastic properties of asphalt mixture.

In recent decades, researchers have conducted several studies to develop the viscoelasticity theory investigating the permanent deformation of flexible pavements. Some previous studies (Masad, Dessouky, and Little 2007; C. W. Huang et al., 2007; Abu Al-Rub, Masad, and Huang 2009) have used Schapery's single integral nonlinear viscoelastic model (Schapery 1969) to analytically predict the recoverable deformation. This model was further developed by some other studies (Abu Al-Rub et al., 2009; Masad et al., 2009) to characterise and decouple the recoverable (viscoelastic) and irrecoverable (viscoplastic) deformations by analysing repeated creep-recoverable experimental tests using Schapery's nonlinear viscoelastic model. On the other hand, to predict the irrecoverable deformations, some studies (Lu and Wright 1998; Seibi et al., 2001) have used the Perzyna's (1971) viscoplastic model. Afterwards, the combination of these models was proposed (W. Huang et al., 2011), and later a damage law was added to these models to

describe the strain response of pavement, considering micro-damages (Darabi et al., 2011). Accordingly, many researchers have shown that the asphalt mixture is a viscoelastic material that has both elastic (i.e., the rigidity of an elastic solid) and viscous behaviours. (i.e., it flows and dissipates energy by frictional losses as a viscous fluid).

Moreover, with the development of advanced computing technologies, promising approaches of finite-element modelling in rutting prediction were reported by many studies (H. Huang 1995; Fang et al., 2007; Hadi Nahi et al., 2014; Gungor et al., 2016). In this regard, one of the finite element nonlinear models that have been successfully validated and frequently and commonly used to characterise the mechanistic behaviour of asphalt mixture is the nonlinear power- or Bailey-Norton-law creep model (Hua 1998; Olsson, Zeng, and Wiberg 2000; White et al., 2002; Fang et al., 2007; Al-Qadi et al., 2009; Arabani, Jamshidi, and Sadeghnejad 2014; Wang et al., 2017; Nguyen et al., 2020). Using this model, the plastic material properties that contribute to the flexible pavements' permanent deformation can be characterised, including a time-dependent accumulation of strains produced by repeated traffic loads.

Typical nonlinear creep behaviour can be divided into primary, secondary, and tertiary stages. With the application of load, the creep strain rate usually decays during the primary stage, and it remains constant at the secondary stage. Creep fracture may occur at the end of the tertiary zone. The wheel-wandering effects can also be considered by simulating the tyre loading time distribution in the pavement's transverse direction through the power-law creep model, confirmed by Hua (1998). For this reason, some recent similar studies (Chen et al., 2016; Chen et al., 2019; Yeganeh et al., 2021; Fahad, Nagy, and Fuleki 2021) simulating the rutting performance of automated vehicles by finite element methods also used power-law creep model to simulate the

material behaviour. To characterize the rutting behaviour of the asphalt layer, this study also used a power-law creep model, shown in Eq. (1).

$$\varepsilon^{cr} = A \times \sigma^{m} \times t^{n} \quad (1)$$

Where ε^{cr} is the creep strain, σ is the stress ($^{N}/_{m^2}$), t is loading time (s), and *A, m*, and *n* are material constants.

The assumed values for parameters *A*, *m,* and *n* are $8.5 \times (10)^{-8}$, -0.75, and 0.8, respectively, obtained from Hua's study (1998). Young's modulus of 3103 MPa and Poisson's ratio of 0.3 were chosen for the elastic material properties.

Moving load model

For modelling a moving load, first, we simulated a single wheel pass on the element sets of the road surface, applying the step load function at the first set of elements and moving in the traffic direction to the next set of elements until completing a single wheel pass. Figure 1 shows this step load function.

[Figure 1 near here]

As can be seen in this figure, the wheel starts its move at the edge of element 1 at time T_0 and covers the entire surface of the element at T_1 and it continues covering the surface of element 1 until time T_2 , and finally leaves the element at time T_3. The duration of time from T_0 to T_1 (i.e., t_1), T_1 to T_2 (i.e., t_2), *and* T_2 to T_3 can be calculated as follows:

$$t_1 = T_1 - T_0 = \frac{a}{v}$$

$$t_2 = T_2 - T_1 = \frac{b}{v} - \frac{a}{v} = \frac{b-a}{v}$$

$$t_3 = T_3 - T_2 = \frac{a+b}{v} - \frac{b}{v} = \frac{a}{v}$$

Where a is the element width, b is the tyre print length, and v is the wheel speed (see Figure 1). Accordingly, the total time duration for a single wheel pass can be calculated as follows:

$$T = t_1 + t_2 + t_3 = \frac{a}{v} + \frac{b-a}{v} + \frac{a}{v} = \frac{a+b}{v}$$

From T_1 to T_2 the load has its maximum value, while from time T_0 to T_1 and from time T_2 to T_3, the total load applied on the surface of element 1 is not at its maximum and varies linearly from zero to maximum and from maximum to zero, respectively. The time duration from T_0 to T_1 equals to that from T_2 to T_3 as the wheel speed is constant. Areas under the load-time plot for these two time intervals are two triangles of the same size. Also, the time duration from T_0 to T_1 or from T_2 to T_3 is much shorter than the time duration from T_1 to T_2. Accordingly, it is assumed that the total effect on element 1 as the wheel load passes from T_0 to T_1 and from T_2 to T_3 can be approximated by the effect of the maximum load being applied for the same time interval. Figure 2 is a schematic demonstration of the detailed transformation of the loading time T. With this assumption, the total loading time T would be equal to $^{b}/_{v}$. Thus, regardless of the size of the element, the total loading time can be calculated by dividing the tyre print length by the speed of the wheel.

[Figure 2 near here]

the accurate prediction of permanent deformation has been challenging due to a large number of load repetitions and the complex nature of vehicular loading conditions and asphaltic material constitutive behaviour (Abu Al-Rub et al., 2012). Despite the computational power of current advanced computers and 3D finite element models, simulation of pavement rutting performance subjected to millions of load applications with realistic wheel wandering and environmental conditions are still challenging. Accordingly, simplified numerical models preserving the efficiency with reasonable loading conditions and material behaviours by considering a large

number of load applications are desirable. Accordingly, to consider the number of load repetition and cyclic moving load, this study used an equivalent loading approach that was first adopted by Huang (1995) and subsequently used by other studies (Hua 1998; Olsson et al., 2000; White et al., 2002; Fang et al., 2007; Al-Qadi et al., 2009; Arabani et al., 2014; Wang et al., 2017; Nguyen et al., 2020). This method could preserve the accuracy and reduce the computational time. In this method, the loading time for each wheel pass is summed up to produce the total cumulative loading time for the elements, which is schematically shown in Figure 3.

[Figure 3 near here]

In the present study, the model is subjected to a dual tyre loading with a tyre contact pressure of 523312 Pa (75.9 psi), uniformly distributed over the tyre and pavement surface contact area. This is assumed to be two rectangles with a length of 0.1981 m and a width of 0.1930 m. The rutting performance of the 5,000 passes of vehicles with the speed of 2.22 m/s with both 2D plane strain and 3D FE models were simulated. Afterward, the FE modelling and the APT results were compared and presented in Table 1. The results are very close, indicating that both 3D and 2D models are reliable for further analysis. The difference in predicted maximum rutting depths between the 3D and 2D plane-strain model is less than 2%, which is not significant. Therefore, in this study, the 2D plane-strain model is used to save computational time in subsequent analyses. In the 2D plane-strain model, the wheel-wander effects can also be considered by simulating the tyre loading time distribution in the transverse pavement direction, confirmed by Hua et al. (1998).

[Table 1 near here]

Simulation of in-service rutting performance

To predict the in-service pavement rutting performance, this study used a full-depth pavement structure with the back-calculated asphalt material property of “9.5 LS 44 Through,

High AC" asphalt mixture, based on the APT facility used in Hua's study (1998). Accordingly, creep constants of A, m, and n are $4.9 \times (10)^{-8}$, -0.715, and 0.8, respectively. The thickness of the full-depth asphalt layer was selected to be 0.5 m. Considering the traffic data used in Zhou et al. (2019), the present study assumed that the pavement structure is subjected to the application of 30 million dual tyre loads (i.e., the model includes two tyres, each receiving a load of 20 kN) within a 20-year design period at a speed of 90 km/h. For the subgrade, infinite elements with linear behaviour were used to model the far-field region. The loading time distributions should be calculated for each evaluation scenario and imported to the FE model to calculate each case's rutting depth profiles and simulate the in-service rutting performance. The following section presents the calculation methods of the loading time distributions for AVs and HDVs.

Wander mode for human-driven vehicles

For simulating the wander distribution of HDVs, the total frequency of vehicle passes was normally distributed. The normal probability distribution function of $f(x)$ can be formulated, as shown in Eq. (2).

$$f(x) = \frac{1}{SD\sqrt{2\pi}} e^{-\frac{1}{2}(\frac{x-\mu}{\sigma})^2} \quad (2)$$

Where μ is a mean value, *SD* is the standard deviation, and x is the offset distance from a reference point.

To determine the empirical standard deviation of normal wander distribution of HDVs ($SD_{empirical}$), which mainly depends on several factors such as driver behaviour, environment, and road characteristics, the present study used the empirical field data of Buiter et al.'s study (1989). In this field study, the standard deviations associated with the normal distribution of

vehicles across the traffic lane were determined using the obtained relevant field data from the tests conducted with a specially developed measuring system. Based on this study's findings, the present work assumed the standard deviations of 0.24, 0.26, and 0.29 m with a respective lane width of 3 m, 3.25 m, and 3.5 m in our study.

To calculate the loading time $t(x)$ for HDVs with a normal wander distribution on any given point x in the road's transverse direction, Eq. (3) could be used as shown in Figure 4 (Hua and White, 2002). In this equation, $t(x)$ is the area under the normal distribution curve within the range of $(x - {}^{w}/_{2})$ to $(x + {}^{w}/_{2})$.

$$t(x) = \left[F\left(x + \frac{w}{2}\right) - F\left(x - \frac{w}{2}\right)\right] \times T \tag{3}$$

Where,

x = offset distance from a reference point

$F(x)$ = normal cumulative distribution for the specified mean and standard deviation

w = tyre width

T = total loading time of the tyre

[Figure 4 near here]

The total loading time (T) is the accumulated repetitions of a single load (Hua, 1998). For this study, a total loading time was determined based on the application of 30 million standard single axle loads with a speed of 25 m/s (90 km/h). The one pass's loading time is 0.007924 seconds, derived by dividing the tyre print length by the wheel speed (0.1981/25 = 0.007924 s). Therefore, the total loading time for 30 million passes would be 237720 seconds (30000000×0.007924).

In the FE method, the load is not applied to a point, but it is applied to an element (edge). With the assumption that the constant load has the same effect as the varying load, Hua and White (2002) proved that as long as the element width is smaller than the tyre width, Eq. (3) can also calculate

the loading time of any surface. For the duel tyres, the total loading time can be calculated by summing (i.e., superposition) the total loading time from each single tyre (Hua and White, 2002). Using Eq. (3) and the superposition method, the transverse loading time distributions for one dual tyre for lane widths of 3 m, 3.25 m, and 3.5 m were calculated, as shown in Figure 5.

[Figure 5 near here]

Wander modes for automated vehicles

This study considers three possible lateral wandering patterns for AVs, naming the "zero-wander", "normal-wander", "uniform-wander" patterns. The uniform-wander mode is calculated in two different formulation approaches (i.e., uniform-time and uniform-frequency). The calculation of loading time distributions for the wander modes mentioned above is presented in the following sections.

Concerning implementing the proposed wander modes for AVs, one could envision individual or cooperative wandering. The AV would swing within the lane in the former approach, following the proposed wander mode. In other words, the vehicle's lateral position would vary for each vehicle as a function of time like HDVs. In the latter approach, the lateral positions of all AVs would be synchronised together (i.e., in truck platooning) so that the lateral position of each vehicle would be fixed but slightly different from others. In other words, the number of AVs driving in each transverse point would finally create the proposed wander-mode for all AVs. In this approach, the assumption is that a large enough number of HDVs and AVs could create the proposed wander modes. In this regard, this study assumed the total number of 30 million vehicles and different evaluation scenarios considering the number of AVs as a percentage of the total number of vehicles (i.e., different AV penetration rates).

Zero-wander mode for automated vehicles

One of the potential wheel-wander distributions for AVs is a zero distribution. In this case, the total loading time is applied simultaneously on two rectangular areas, regardless of the lane width. As mentioned above, the one pass's loading time is 0.007924 s, and the accumulated repetitions of the single load would result in the total loading time. Considering the total of 30 million vehicle passes for the combination of AVs and HDVs, the total loading time imposed by AVs for the penetration rates of 0%, 20%, 40%, 60%, 80%, and 100% would be 0 s, 47544 s, 95088 s, 142632 s, 190176 s, and 237720 s, respectively. The loading time of each transverse point for the mixed traffic scenarios is calculated by summating the loading time imposed by AVs and the one imposed by HDVs in each transverse point, considering the AVs' penetration rates. Figure 6 shows the loading time distribution for the mixed traffic of HDVs with normal-wander mode and AVs with zero-wander mode with different penetration rates for each lane width.

[Figure 6 near here]

Normal-wander mode for automated vehicles

Considering the AVs' programmable capabilities, AVs could also be programmed to follow a normal distribution with a predetermined theoretical standard deviation ($SD_{Theoretical}$). The determination of $SD_{Theoretical}$ depends on the lane's available space for wheel-wander (i.e., wandering width) and the assumed confidence interval for the normal distributions. The wandering width could be calculated by subtracting the truck width from the lane width. The width of an 18-wheel standard truck is approximately 2.59 m (8.5 ft.). Accordingly, the wandering width for the lane widths of 3 m, 3.25 m, and 3.5 m would be 0.41 m, 0.66 m, and 0.91 m, respectively. To determine the confidence interval, this study assumed the values less than three standard deviations away from the mean ($\mu \pm 3SD_{Theoretical}$), accounting for 99.7% of the vehicles. Thus, the

$SD_{Theoretical}$ can be calculated by dividing the wandering width by six. Accordingly, the $SD_{Theoretical}$ for lane widths of 3 m, 3.25 m, and 3.5 m are 0.07, 0.11, and 0.15, respectively. After distributing the vehicle frequencies with normal distribution, the loading time of each transverse point could be calculated, using Eq. (3), where the $F(x)$ is the normal cumulative distribution with the standard deviation of $SD_{Theoretical}$. Figure 7 shows the loading time distribution for the mixed traffic of HDVs with normal-wander mode (i.e., with $SD_{empirical}$), and AVs with normal-wander mode (i.e., with $SD_{Theoretical}$) with different penetration rates for each lane width.

[Figure 7 near here]

Uniform-wander mode for automated vehicles

The other potential wheel-wander distribution for AVs is a uniform distribution. The uniform distribution is constant over a given width interval, bounding by the parameters *a* and *b*, which are the minimum and maximum values. Accordingly, from *a* to *b*, where $a < b$, the uniform function forms as Eq. (4).

$$f(x) = \begin{cases} \frac{1}{b-a}, & a \le x < b \\ 0, & otherwise \end{cases} \tag{4}$$

This study considers two approaches to formulate and implement a uniform wander distribution for the AVs; uniform-time and uniform-frequency, presented in the following sub-sections.

Uniform-time approach

In the uniform-time approach, the vehicle's lateral movement pattern is programmed so that the loading time of all transverse points of x within the loading span of *a* to *b* would be equal. In this case, to calculate the loading span, the truck width is subtracted from the lane width, and then,

the loading span is extended by half of the dual tyre width from each side to consider the complete contact area between the tyres and the pavement. Accordingly, the loading span for lane widths of 3 m, 3.25 m, and 3.5 m are 0.94 m, 1.19 m, and 1.44 m, respectively (i.e., the boundary values with reference to the centre of the dual tyre ($x = 0$) are -0.47 to 0.47, -0.59 to 0.59, and -0.72 to 0.72, respectively). Accordingly, the total loading time was distributed uniformly on the remaining available space for the wheels. Figure 8 shows the loading time distribution for the mixed traffic of HDVs with normal-wander mode and AVs with uniform-time-wander mode with different penetration rates for each lane width.

[Figure 8 near here]

Uniform-frequency approach

In the uniform-frequency approach, the vehicle pass frequencies are distributed uniformly within the available width of the road lane. Considering the centre of a dual tyre as a reference point for a vehicle pass, the remaining space for the vehicle passes is derived by subtracting the truck's width from the lane width. Considering the truck width of 2.59 m, the wandering space for lane widths of 3 m, 3.25 m, and 3.5 m are 0.41 m, 0.66 m, and 0.91 m, respectively. For instance, for the lane width of 3 m, each point of a tyre can move 0.205 m (0.41/2) to the left or right. The distance between the centres of the tyres is 0.335 m. This study assumed the centre of the dual tyre as a reference point (x = 0). Accordingly, the centre of the right tyre is +0.167 m, and the centre of the left tyre is -0.167 m. Thus, by distributing the frequency of vehicle passes uniformly, the values of a and b for the uniform distribution for the right tyre are -0.038 and 0.372, respectively, and for the left tyre are -0.372 and 0.038, respectively. After distributing the vehicle frequencies uniformly, the loading time of each transverse point could be calculated, using Eq. (4), where the $F(x)$ is the uniform cumulative distribution for the specified a and b values. Therefore, the

loading time of an element with a distance of x from the center of the lane is equal to the area under the uniform distribution function within the range of $(x - {}^{w}/_{2})$ to $(x + {}^{w}/_{2})$. By the summation (i.e., superposition) of the loading time of each point for the left and right tyre of the dual tyre, the transverse loading time distributions for one dual tyre were calculated. Figure 9 shows the loading time distribution for the mixed traffic of HDVs with normal-wander mode and AVs with uniform-frequency-wander mode with different penetration rates for each lane width.

[Figure 9 near here]

Results

The pavement rutting FE simulations for one dual tyre with 30 million vehicle passes and a speed of 25 m/s (90 km/h) were performed on the full-depth pavement structure for all scenarios, and the in-situ total rutting depths were determined. Figure 10 shows the total rutting depth in all scenarios and demonstrates the increase or decrease of the total rutting depth by increasing the AVs' penetration rate. As shown in this figure, in the reference scenarios, when there are only HDVs with the normal-wander distribution on the road lane (i.e., 0% AVs or reference scenario), the total rutting depths for the lane widths of 3 m, 3.25 m, and 3.5m are 35.36 mm, 33.47 mm, and 30.77 mm, respectively. As can be seen, in all scenarios except the uniform-time-wander mode, there is a steady increase in the total rutting depth when the AVs' penetration rates rise from 0% to 80%. This rise is followed by a substantial increase when the penetration rate increases from 80% to 100%. However, by increasing the AVs' penetration rate in the uniform-time-wander mode from 0% to 80%, the total rutting depth has an initial decrease, followed by a steady increase. In the lane width of 3 m, the minimum rutting depth in the uniform-time-wander mode is observed in the 20% penetration rate; however, the minimum total rutting for the lane width of 3.25 m and 3.5 m depth is observed at the 60% penetration rate. Furthermore, like the other wander modes,

there is a significant increase in the total rutting depth of the uniform-time-wander mode by increasing the AVs' penetration rate from 80% to 100%.

[Figure 10 near here]

Wander mode effect

Comparing the rutting simulation results of zero-, normal-, uniform-time-, uniform-frequency-wander modes for AVs showed that the total rutting depth induced by the uniform-time-wander mode is lower than the one induced by the other wander modes in all the scenarios. Figure 11 shows the wander mode effect on the total rutting depth in all scenarios and demonstrates the percentage of the decreased total rutting depth in the uniform-time-wander mode compared to the zero-wander mode. Moreover, as shown in Figure 11, the differences between the total rutting depth induced from different wander modes get more significant by increasing the AVs penetration rate. For instance, in the lane width of 3.5 m and 20% AVs, using uniform-time-wander mode for AVs resulted in 8.69% lower rutting depth than the zero-wander mode's rutting. However, in the case of 100% AVs, this difference is 27.36%.

[Figure 11 near here]

Lane width effect

The results showed that the total rutting depth in narrower lanes is higher than the wider lanes in all the cases. However, the simulation results with different AVs' penetration rates revealed that the significance of the lane width effect on the total rutting depths is not similar for different wander modes and in different penetration rates. As shown in Figure 12, when using the zero-wander mode for AVs, by increasing the AVs' penetration rates, the differences between the total rutting depths in the given lane widths get smaller so that in the case of 20% AVs, the rutting value

for the 3 m lane is 14.92% higher than the one for the 3.5 m lane, and this difference reaches 0% in the case of 100% AVs. Inversely, when using uniform-time-wander mode for AVs, the lane width effect on the total rutting depth gets more significant at the higher AVs' penetration rates so that in the case of 100% AVs, the total rutting depth for a lane width of 3 m is 25.04% higher than the one for 3.5 m. Furthermore, in the case of using normal- or uniform-frequency for the AVs, the difference percentage between the rutting values of the different lane widths are almost the same for the mixed traffic scenarios. However, in the segregated scenario with 100% AVs, this difference gets more substantial. For instance, in the case of using uniform-frequency-wander mode in the mixed traffic scenarios (i.e., 20%, 40%, 60%, and 80% AVs), the difference between the rutting values of 3 m lane and 3.5 m lane are ranged from 14% to 15%. However, in the segregated scenario with 100% AVs, this difference is 18.16%.

[Figure 12 near here]

Discussion

The present study was designed to enhance the current understanding of the AVs' implications on the pavement rutting performance by examining the wander mode effects with different penetration rates and the lane width effects. The following sections, first, discuss the implication of zero-, normal-, uniform-time-, and uniform-frequency-wander modes for AVs individually and compare them with the reference scenario. Afterward, discuss and compare the implication of different wander modes, and finally, discuss the limitation and future works.

Zero- and normal-wander mode implication

The AVs could have no lateral wandering (except for very negligible movement due to potential wind load), which leads them to follow a single track in the centre of the lane. In this

regard, one of the possible preliminary options for the AVs' lateral wandering, which has been investigated in the previous studies (Chen et al., 2016; Noorvand and Underwood, 2017; Chen et al., 2019), is a zero-wander distribution mode. These studies concluded that AVs' zero-wander distribution could accelerate the pavement rutting damage compared with the HDVs' normal distribution. Our study's results further supported this understanding. Accordingly, by increasing the AVs' penetration rates, the total rutting depth increased.

One of the other potential wander modes for AVs simulated in this study is the normal-wander mode with predetermined theoretical standard deviations for different lane widths. Using normal-wander mode for AVs would accelerate the rutting damage compared with the reference scenario with 0% AVs, and the rutting value is significantly higher in the segregated scenarios with 100% AVs compared with the mixed traffic scenarios.

The other finding of our study, which has not been investigated in previous studies and can develop our understanding of the zero-wander performance, is that the differences between the total rutting depth in the lane widths of 3 m, 3.25 m, and 3.5 m are more considerable in the lower penetration rates compared to higher penetration rates (see Figure 12). Thus, this has significant practical implications meaning that although using a zero-wander mode for AVs in higher penetration rates would result in a higher rutting depth compared to the case of 100% HDVs (i.e., reference scenarios), the additional negative impact of using a narrower lane is less substantial when compared to the wider lanes.

Therefore, generally, the results of this study do not recommend using the zero- and normal-wander mode (i.e., with $SD_{Theoretical}$) for AVs in none of the cases. Nonetheless, this study could recommend using narrower lanes to save construction and maintenance costs if choosing the zero-wander mode for the AVs with higher penetration rates. However, the findings of this study could

not recommend using narrower lanes for AVs with the normal-wander mode in none of the penetration rates because it would result in a significantly higher rutting value than the wider lanes.

Concerning the implication of normal-wander mode for AVs, it is worth mentioning that the most remarkable difference between AVs and HDVs is AVs' programmable steering capability, which enables different controlled lateral movement patterns. The lateral movement patterns of HDVs depend on several factors such as driver, environment, and road characteristics. Accordingly, these lateral movements are calculated using empirical field data, not theoretical calculations. In reality, HDVs may tend to cross the edge or centre lines and, hence, have wider wandering (i.e., larger standard deviations of lateral position). On the contrary and for AVs, their lateral movement should be programmed in a way that they may not override the lane markings. Thus, the calculated standard deviations for AVs in the present study are significantly smaller than the empirically retrieved ones for HDVs. Consequently, the rutting depth induced by the normal-wander mode of AVs is considerably higher than that of HDVs. The smaller standard deviations of AVs would confine them not to exceed the lane markings (unlike the HDVs) and could cause less collisions (specifically head-on collisions) and, therefore, a safer situation is achieved.

Uniform-wander mode implication

Some previous studies (Noorvand and Underwood, 2017; Chen et al., 2019; Zhou et al., 2019) took advantage of AVs' programmable steering control systems to suggest a uniform-wander distribution as a more proper lateral wandering pattern for AVs. However, our study's observations on uniform mode do not fully support this view for all possible cases. As previously discussed, this study considers two possible approaches of uniform-time and uniform-frequency for the implication of uniform-wander mode. The simulation results of these two approaches are discussed in the following sections.

Uniform-time-wander mode implication

The findings of our study showed that the application of AVs up to 80% on the road pavements with the uniform-time-wander mode has not a significant impact (i.e., less than 2.66% in the worst-case scenario) on the total rutting depth. However, with the application of 100% AVs with the uniform-time-wander mode, the total rutting depth has been significantly increased compared to the reference scenarios and mixed traffic scenarios.

This study added another critical finding to the current understanding of the uniform-wander mode by considering the lane width effects. Our findings showed that the lane width effect is more significant in the higher AVs' penetration rates for the uniform-time wander mode (see Figure 12), which was the other way around in the zero-wander cases. A practical implication of this could be that the presence of a narrower lane for AVs with the uniform-time wander mode in the higher penetration rates would cause significant additional adverse effects on pavement life compared to the wider lanes and, thus, there is a need to widen the lanes to enhance the pavement life. However, in the transition era, when the AVs' penetration rates are still low, the adverse effects of using narrower lanes are less significant compared to the higher penetration rate scenarios, and there might be no need to widen the lanes until reaching a certain point of penetration rate. Nevertheless, further investigations need to compare the benefits of using narrower lanes like saving space and construction and maintenance costs with the negative impacts of using the narrower lane on the pavement rutting performance.

Uniform-frequency-wander mode implication

The results showed that, in the uniform-frequency-wander mode scenarios, the application of AVs from 0% to 80% penetration rate (i.e., mixed traffic) could increase the pavement rutting depth up to 3.69% in the worst-case scenario, which is not significant. However, in the segregated

scenario with 100% AVs, the total rutting depth is significantly higher than the reference and mixed traffic scenarios. Moreover, it is observed that the significance of the lane width effect on rutting performance in the mixed traffic scenarios (i.e., in the penetration rates of 20%, 40%, 60%, and 80%) is almost constant so that the total rutting depth in the lane width of 3.5 m is about 14% lower than the one in the 3 m lane. Nevertheless, the significance of lane width effect on rutting performance is more than the mixed traffic scenarios, so that the difference between rutting values of 3 m lane and 3.5 m lane is 18.16%.

The points discussed above regarding the uniform-wander mode scenarios could have a practical implication meaning that in the near future (i.e., the transition era from HDVs to AVS), when the AVs penetration rate is still low, using both uniform-time- and uniform-frequency-wander modes would not have a significant positive or negative impact on the pavement rutting performance. Thus, AVs' uniform-wander mode could be used to avoid the potential accelerated rutting damage of the flexible pavements induced by other wander modes like zero and normal distributions.

Comparison between the implication of different wander modes

Comparing the rutting performance of zero- and uniform-wander effects in the previous studies (Noorvand and Underwood, 2017; Chen et al., 2019; Zhou et al., 2019) showed that a uniform-wander mode has a smaller total rutting depth than the zero-wander mode. Our study could further support this argument considering both uniform-time and uniform-frequency approaches in all scenarios. In addition, the findings of this study showed that in all scenarios, the application of the uniform-time wander mode would result in lower rutting depth compared to the uniform-frequency- and normal-wander modes. Another remarkable finding of this study is that the significance of the wander mode effect is more considerable in the higher penetration rates

compared with lower penetration rates, and it is also more considerable in the wider lanes compared with narrower lanes.

Comparing the rutting performance of different wander modes discussed above suggests several important implications for future practice and policy. Automated vehicles could benefit from their programmable capabilities to adapt their lateral movement pattern to the existing lane widths and different penetration rates to enhance the pavement rutting performance. Although in all scenarios, the rutting performance induced from uniform-time-wander mode is better than the other wander modes, in some cases, like lower penetration rates or narrower lanes, the differences between the rutting values of different wander modes are not significant. In these cases, choosing the wander mode that is practically more applicable would need less demanding technologies and save potential extra costs. From this perspective, the technology needed to design the zero-wander mode for AVs might be less demanding than the other wander patterns in practical terms or designing the uniform-frequency wander mode might be more applicable than the uniform-time-wander mode. In this sense, the AVs could adapt their wander mode to the more applicable and cost-effective ones based on the existing scenario. For instance, when AVs detect a narrower lane, the uniform-frequency-wander mode could be more applicable without any significant additional adverse effect on pavement rutting performance than the uniform-time-wander mode. In some cases, like the lane width of 3 m and the penetration rates of 20% AVs, even using zero-wander mode could be more applicable with only 4.25% additional rutting depth.

Limitations and future works

The points discussed above demonstrated that with the emergence of AVs on the roads, the pavement damage could be significantly influenced by the different lane-management scenarios. This necessitates further research on the economic assessment and life cycle cost analysis for AVs.

For instance, the cost analysis of increased pavement rutting depth induced by AVs in some cases and the benefits of saving construction and maintenance costs resulted from using narrower lanes would provide constructive conclusions in this area. Moreover, the technologies and costs needed to design different wander modes for AVs and the feasibility of the application of each wander mode need to be investigated.

The combinations of these findings contribute to our knowledge of AVs' implications on the pavement rutting performance and the decision-making process on the choice of lateral wandering patterns for AVs in different lane distribution scenarios. However, several important limitations should be considered.

- The rutting profile could have a "feedback-loop" effect on the actual positioning of the vehicles. In other words, the tyre tracks created by the time in the rutting profile could attract the tyres, which leads to less wandering and would affect the wander distribution of the vehicles. The simulations performed in this study have not taken this feedback effect into account.
- Concerning the safety issues, comprehensive and independent research needs to be performed to study the traffic safety implications of different wander modes for mixed traffic scenarios. Moreover, it is essential to study the necessity of considering safety distance for AVs and their effects on different aspects of the transportation system and operations. This could have significant practical implications meaning that road designers might not consider extremely narrow lane widths, given the adverse effects that this could bring about as a result of incorporating the safety distance in the AVs' manoeuvring programmes.

- This study considered only one pavement structure and material to simulate the rutting performance. Hence, future research is worth exploring different asphalt mixtures and thicknesses.

Conclusions

Based on the simulation results and the evaluation of rutting performance, the following conclusions can be drawn:

- The rutting damage caused by a segregated scenario with 100% AVs is significantly higher than the one caused by mixed traffic scenarios in all wander modes and lane widths. Thus, using shared lanes for AVs and HDVs could contribute to enhancing the pavement rutting life.
- Two approaches presented in this study for the formulation of the uniform-wander mode (i.e., uniform-time and uniform-frequency) provided us with a better insight into the implication of wander mode for AVs. Accordingly, the implication of both uniform-time and uniform-frequency modes for AVs in all penetration rates and lane widths scenarios would result in lower rutting damage than one induced by the other evaluated wander modes. Hence, using a uniform-wander mode for AVs could avoid the potential accelerated damage caused by the AVs' initial tendency to keep lane-centring within the road lanes.
- In the zero-wander mode, the variations between the total rutting depth in different lane widths are more considerable in lower penetration rates than higher penetration rates. In this case, the additional negative impact of using a narrower lane is less substantial when having higher penetration rates. Accordingly, if the policymakers decide to use this mode as the default wandering mode for AVs due to its simplicity, this study would

recommend using narrower lanes in the higher penetration rates to save construction and maintenance costs.

- In the uniform-time-wander mode, the lane width effect on rutting performance is less significant in lower AVs' penetration rates than higher ones. Thus, the adverse effects of using narrower lanes are less significant in lower penetration rates in the uniform-time-wander mode. For this reason, using narrower lanes could be a reasonable option for designers in the transition era (i.e., when the AVs' penetration rates are still low). However, this study could warn that there might be a need to widen the lanes after reaching a certain penetration rate. This necessitates the economic comparison between the benefits of using narrower lanes (e.g., saving space and construction and maintenance costs) and the negative impacts of using the narrower lane on the pavement rutting performance.
- The gradual introduction of AVs with uniform-time-wander mode could decrease the total rutting value until a certain level of penetration rate. The total rutting depth would increase significantly upon reaching a certain penetration rate. This turning point is not observed at the same penetration level for different lane widths. For instance, in the lane width of 3 m, the minimum rutting depth is observed in the case of 20% AVs while in the lane width of 3.5 m, the minimum rutting depth is observed in the case of 60% AVs. Thus, practically, using narrower lanes dismiss the opportunity to benefit from the reduced rutting depth caused by uniform-time-wander mode from early lower penetration rates.
- In the normal- and uniform-frequency-wander modes for AVs, the variations between the total rutting depth in different lane widths are more considerable in the dedicated

lanes (i.e., 100% AVs) compared with the shared lanes. In this case, using a dedicated narrower lane for AVs could significantly increase the rutting damage.

- This study's findings provided a possibility of comparing different AVs' distribution scenarios with each other and the potential practical implications for each level of AVs' penetration rate were discussed. The rutting performance of the evaluated scenarios indicated that the significance level of the wander mode, penetration rates, and lane width effect on the rutting damage is dependent on each other, and it is essential to consider their effects simultaneously to better evaluate the pavement rutting performance in the era of co-existence of AVs and HDVs on the roads. Accordingly, the findings of this study showed that the AVs' penetration rate is crucial in policymaking regarding AVs' steering control system design, lane distribution for AVs and HDVs, and the widening or narrowing of the road lanes.

Declaration interest

Declarations of interest: none

Acknowledgments

We would like to express our great appreciation to Amir Hossain Mohammadi, for his valuable and constructive suggestions and helpful comments during the development of this research work's finite element model.

References

Abu Al-Rub, R. K., Masad, E. A. and Huang, C.-W. (2009) 'Improving the Sustainability of Asphalt Pavements through Developing a Predictive Model with Fundamental Material

Properties', *Swutc/09/476660-00007-1*, 1(2), p. 59.

Al-Qadi, I. L. et al. (2009) 'Creep behavior of hot-mix asphalt due to heavy vehicular tire loading', *Journal of Engineering Mechanics*, 135(11), pp. 1265–1273. doi: 10.1061/(ASCE)0733-9399(2009)135:11(1265).

Ali, B., Sadek, M. and Shahrour, I. (2008) 'Elasto-viscoplastic finite element analysis of the long-term behavior of flexible pavements application to rutting', *Road Materials and Pavement Design*, 9(3), pp. 463–479. doi: 10.3166/rmpd.9.463-479.

Amirgholy, M., Shahabi, M. and Oliver Gao, H. (2020) 'Traffic automation and lane management for communicant, autonomous, and human-driven vehicles', *Transportation Research Part C: Emerging Technologies*. Elsevier, 111(November 2019), pp. 477–495. doi: 10.1016/j.trc.2019.12.009.

Arabani, M., Jamshidi, R. and Sadeghnejad, M. (2014) 'Using of 2D finite element modeling to predict the glasphalt mixture rutting behavior', *Construction and Building Materials*. Elsevier Ltd, 68, pp. 183–191. doi: 10.1016/j.conbuildmat.2014.06.057.

Binshuang, Z. et al. (2019) 'Skid resistance demands of asphalt pavement during the braking process of autonomous vehicles', *MATEC Web of Conferences*, 275(January), p. 04002. doi: 10.1051/matecconf/201927504002.

Buiter, R. et al. (1989) 'Effects of transverse distribution of heavy vehicles on thickness design of full-depth asphalt pavements', *Transportation Research Record*, (1227), pp. 66–74.

Burgers, J. M. (1935) *First and second report on viscosity and plasticity*. the Netherlands: Academy of Sciences at Amsterdam.

Chen, F. et al. (2019) 'Assess the impacts of different autonomous trucks' lateral control modes on asphalt pavement performance', *Transportation Research Part C: Emerging Technologies*.

Elsevier, 103(March), pp. 17–29. doi: 10.1016/j.trc.2019.04.001.

Chen, F., Balieu, R. and Kringos, N. (2016) 'Potential Influences on Long-Term Service Performance of Road Infrastructure by Automated Vehicles', *Transportation Research Record: Journal of the Transportation Research Board*, 2550(1), pp. 72–79. doi: 10.3141/2550-10.

Chen, F., Song, M. and Ma, X. (2020) 'A lateral control scheme of autonomous vehicles considering pavement sustainability', *Journal of Cleaner Production*, 256. doi: 10.1016/j.jclepro.2020.120669.

Darabi, M. K. et al. (2011) 'A thermo-viscoelastic-viscoplastic-viscodamage constitutive model for asphaltic materials', *International Journal of Solids and Structures*, 48(1), pp. 191–207. doi: 10.1016/j.ijsolstr.2010.09.019.

Erlingsson, S. (2004) 'Mechanistic Pavement Design Methods – A Road to Better Understanding of Pavement Performance', *Via Nordica 2004 – NRA's 19th Road Congress, C8: Berekraftige vegkonstruksjonar*, (June 2014), pp. 1–8. Available at: https://www.researchgate.net/publication/242219834_Mechanistic_Pavement_Design_Methods_-_A_Road_to_Better_Understanding_of_Pavement_Performance.

Fahad, M., Nagy, R. and Fuleki, P. (2021) 'Creep model to determine rut development by autonomous truck axles on pavement', *Pollack Periodica*, pp. 1–6. doi: 10.1556/606.2021.00328.

Fang, H. et al. (2007) 'An object-oriented framework for finite element pavement analysis', *Advances in Engineering Software*, 38(11–12), pp. 763–771. doi: 10.1016/j.advengsoft.2006.08.045.

G. Mayorga, M. et al. (2016) , *Journal of Chemical Information and Modeling*, 6(2), pp. 1689–1699. doi: 10.1017/CBO9781107415324.004.

Gungor, O. E. et al. (2016) 'In-situ validation of three-dimensional pavement finite element models', in *The Roles of Accelerated Pavement Testing in Pavement Sustainability: Engineering, Environment, and Economics*. doi: 10.1007/978-3-319-42797-3_10.

Gungor, O. E. and Al-Qadi, I. L. (2020a) 'All for one: Centralized optimization of truck platoons to improve roadway infrastructure sustainability', *Transportation Research Part C: Emerging Technologies*. Elsevier, 114(February), pp. 84–98. doi: 10.1016/j.trc.2020.02.002.

Gungor, O. E. and Al-Qadi, I. L. (2020b) 'Wander 2D: a flexible pavement design framework for autonomous and connected trucks', *International Journal of Pavement Engineering*. Taylor & Francis, 0(0), pp. 1–16. doi: 10.1080/10298436.2020.1735636.

Hadi Nahi, M. et al. (2014) 'Finite Element Model for Rutting Prediction in Asphalt Mixes in Various Air Void Contents', *Journal of Applied Sciences*, 14(21), pp. 2730–2737. doi: 10.3923/jas.2014.2730.2737.

Hua, J. (1998) *Finite element modeling and analysis of accelerated pavement testing device and rutting phenomenon*.

Hua, J. and White, T. (2002) 'A Study of Nonlinear Tire Contact Pressure Effects on HMA Rutting', *The International Journal of Geomechanics*, 2(May 2001), p. 45. doi: 10.1061/(ASCE)1532-3641(2002)2.

Huang, C. W. et al. (2007) 'Nonlinearly viscoelastic analysis of asphalt mixes subjected to shear loading', *Mechanics of Time-Dependent Materials*, 11(2), pp. 91–110. doi: 10.1007/s11043-007-9034-5.

Huang, H. (1995) *Analysis of accelerated pavement tests and finite element modeling of rutting phenomenon*. Purdue University by Haiming Huang.

Kuo, C. M. and Chou, F. J. (2011) 'Journal of the Chinese Institute of Engineers Development of

3D finite element model for flexible pavements', *Journal of the Chinese Institute of Engineers*, 27(May 2015), pp. 37–41. doi: 10.1080/02533839.2004.9670918.

Liu, Z. and Song, Z. (2019) 'Strategic planning of dedicated autonomous vehicle lanes and autonomous vehicle/toll lanes in transportation networks', *Transportation Research Part C: Emerging Technologies*. Elsevier, 106(March), pp. 381–403. doi: 10.1016/j.trc.2019.07.022.

Lu, Y. and Wright, P. J. (1998) 'Numerical approach of visco-elastoplastic analysis for asphalt mixtures', *Computers and Structures*, 69(2), pp. 139–147. doi: 10.1016/S0045-7949(98)00139-4.

Masad, E. et al. (2009) 'Characterization of Asphalt Binder Resistance to Permanent Deformation Based on Nonlinear Viscoelastic Analysis of Multiple Stress Creep Recovery (MSCR) Test', in.

Masad, E., Dessouky, S. and Little, D. (2007) 'Development of an Elastoviscoplastic Microstructural-Based Continuum Model to Predict Permanent Deformation in Hot Mix Asphalt', *International Journal of Geomechanics*, 7(2), pp. 119–130. doi: 10.1061/(asce)1532-3641(2007)7:2(119).

Maxwell, J. C. (1867) 'On the Dynamical Theory of Gases', *Philosophical Transactions of the Royal Society of London*. The Royal Society, 157, pp. 49–88. Available at: http://www.jstor.org/stable/108968.

McCullah, J. and Gray, D. (2005) *Cooperative Highway Program*.

Mohajerpoor, R. and Ramezani, M. (2019) 'Mixed flow of autonomous and human-driven vehicles: Analytical headway modeling and optimal lane management', *Transportation Research Part C: Emerging Technologies*. Elsevier, 109(November), pp. 194–210. doi: 10.1016/j.trc.2019.10.009.

Nguyen, V. B. et al. (2020) 'Creep behavior and rutting resistance of asphalt pavements by

experimental testing and Finite Element modelling', in Ha-Minh, C. et al. (eds) *CIGOS 2019, Innovation for Sustainable Infrastructure*. Singapore: Springer Singapore, pp. 621–626.

Noorvand, H. and Underwood, B. S. (2017) 'Hossein Noorvand, B. Shane Underwood, Arizona State University, Tempe, AZ 85287, USA', *Transportation Research Record*, 2640, pp. 21–28. doi: 10.3141/2640-03.

Olsson, J., Zeng, L. and Wiberg, N. E. (2000) 'Finite element analysis of road rutting', *European Congress on Computational Methods in Applied Sciences and Engineering, ECCOMAS 2000*, (September), pp. 11–14.

Perl, M., Uzan, J. and Sides, A. (1983) 'Visco-Elasto-Plastic Consititutive Law for a Bituminous Mixture Under Repeated Loading.', *Transportation Research Record*, 47(I), pp. 20–27.

Perzyna, P. (1971) 'Thermodynamic Theory of Viscoplasticity', *Advances in Applied Mechanics*, 11(C), pp. 313–354. doi: 10.1016/S0065-2156(08)70345-4.

Rana, M. M. and Hossain, K. (2021) 'Simulation of autonomous truck for minimizing asphalt pavement distresses', *Road Materials and Pavement Design*, pp. 1–21. doi: 10.1080/14680629.2021.1883469.

Razmi Rad, S. et al. (2020) 'Design and operation of dedicated lanes for connected and automated vehicles on motorways: A conceptual framework and research agenda', *Transportation Research Part C: Emerging Technologies*. Elsevier, 117(October 2019), p. 102664. doi: 10.1016/j.trc.2020.102664.

Saevarsdottir, T. and Erlingsson, S. (2015) 'Modelling of responses and rutting profile of a flexible pavement structure in a heavy vehicle simulator test', *Road Materials and Pavement Design*, 0629. doi: 10.1080/14680629.2014.939698.

Schapery, R. A. (1969) 'On the characterization of nonlinear viscoelastic materials', *Polymer*

Engineering & Science, 9(4), pp. 295–310. doi: 10.1002/pen.760090410.

Seibi, A. C. et al. (2001) 'Constitutive relations for asphalt concrete under high rates of loading', *Transportation Research Record*, (1767), pp. 111–119. doi: 10.3141/1767-14.

Siddharthan, R. V. et al. (2017) 'Investigation of impact of wheel wander on pavement performance', *Road Materials and Pavement Design*, 18(2), pp. 390–407. doi: 10.1080/14680629.2016.1162730.

Smith, M. (2009) 'ABAQUS/Standard User's Manual, Version 6.9.' Dassault Systèmes Simulia Corp, Providence, RI.

Song, M., Chen, F. and Ma, X. (2021) 'Organization of autonomous truck platoon considering energy saving and pavement fatigue', *Transportation Research Part D: Transport and Environment*. Elsevier Ltd, 90(December 2020), p. 102667. doi: 10.1016/j.trd.2020.102667.

Timm, D. and Priest, A. (2005) 'Measurement of Wheel Wander Under Live Traffic Conditions', *7th International Conference on the Bearing Capacity of Roads, Railways and Airfields (BCRA'05)*.

Voigt, W. (1892) 'Ueber innere Reibung fester Körper, insbesondere der Metalle', *Annalen der Physik*, 283, pp. 671–693.

W. Huang, C. et al. (2011) *Three-Dimensional Simulations of Asphalt Pavement Permanent Deformation Using a Nonlinear Viscoelastic and Viscoplastic Model*, *Journal of Materials in Civil Engineering*. doi: 10.1061/(asce)mt.1943-5533.0000022.

Wang, Y. et al. (2017) 'Finite element analysis for rutting prediction of asphalt concrete pavement under moving wheel load', *International Journal of Simulation Modelling*, 16(2), pp. 229–240. doi: 10.2507/IJSIMM16(2)4.374.

White, T. D. et al. (2002) *Contributions of Pavement Structural Layers to Rutting of Hot Mix*

Asphalt Pavements, NCHRP Report 468, *Transportation Research Board and American Association of State Highway and Transportation Officials*.

Yeganeh, A., Vandoren, B. and Pirdavani, A. (2021) 'Impacts of Load Distribution and Lane Width on Pavement Rutting Performance for Automated Vehicles', *International Journal of Pavement Engineering*. doi: 10.1080/10298436.2021.1935938.

Zhou, F. et al. (2019) 'Optimization of Lateral Wandering of Automated Vehicles to Reduce Hydroplaning Potential and to Improve Pavement Life', *Transportation Research Record*, pp. 1–9. doi: 10.1177/0361198119853560.

Table 1 Comparison between the 2D and 3D FE models and the APT

Rutting mode	2D model	3D model	APT	The ratio of 2D/APT	The ratio of 3D/APT	The ratio of 2D/3D
Maximum compressive rutting (mm)	1.478	1.464	1.473	1.003	0.994	1.010
Maximum uplift rutting (mm)	1.661	1.662	1.701	0.976	0.977	0.999

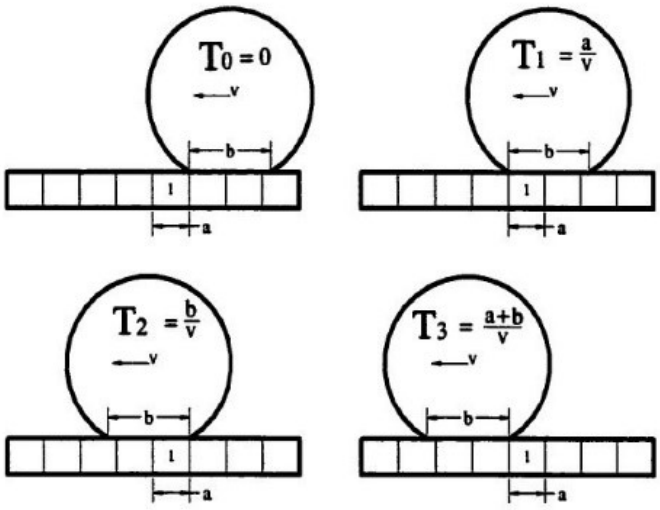

Figure 1 Step loading time calculation (Hua, 1998)

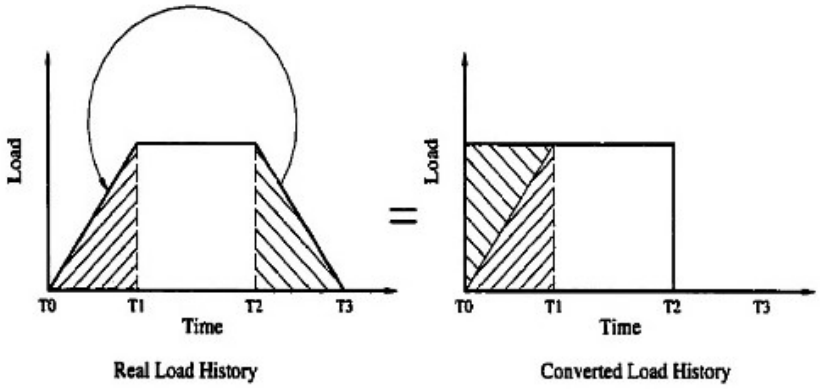

Figure 2 Load duration conversion (Hua, 1998)

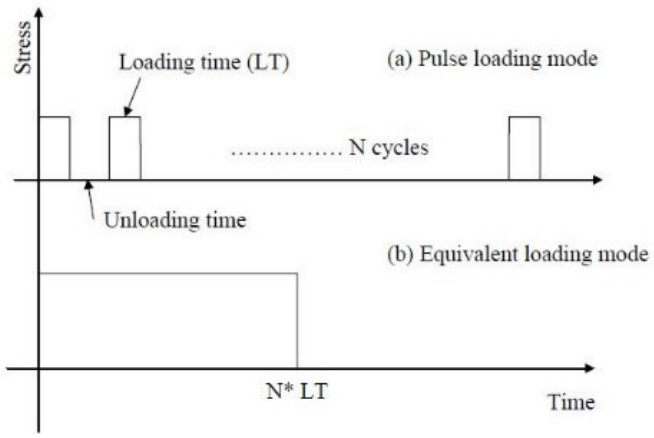

Figure 3 Equivalent loading model (Abu Al-Rub et al., 2012)

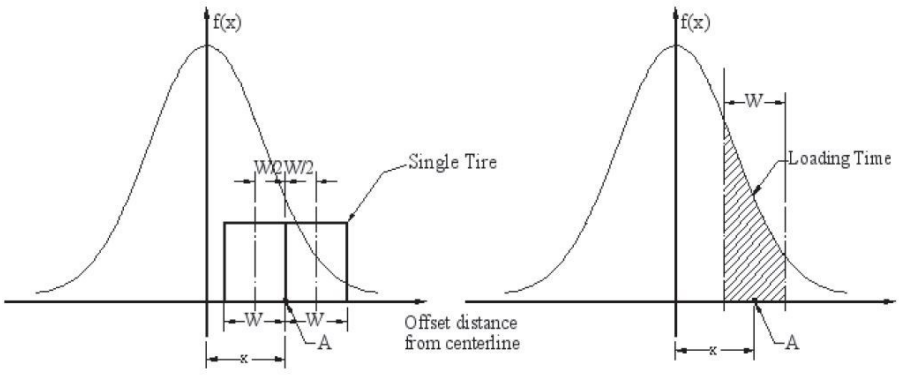

Figure 4 Loading time for any point on the pavement surface (Hua and White, 2002)

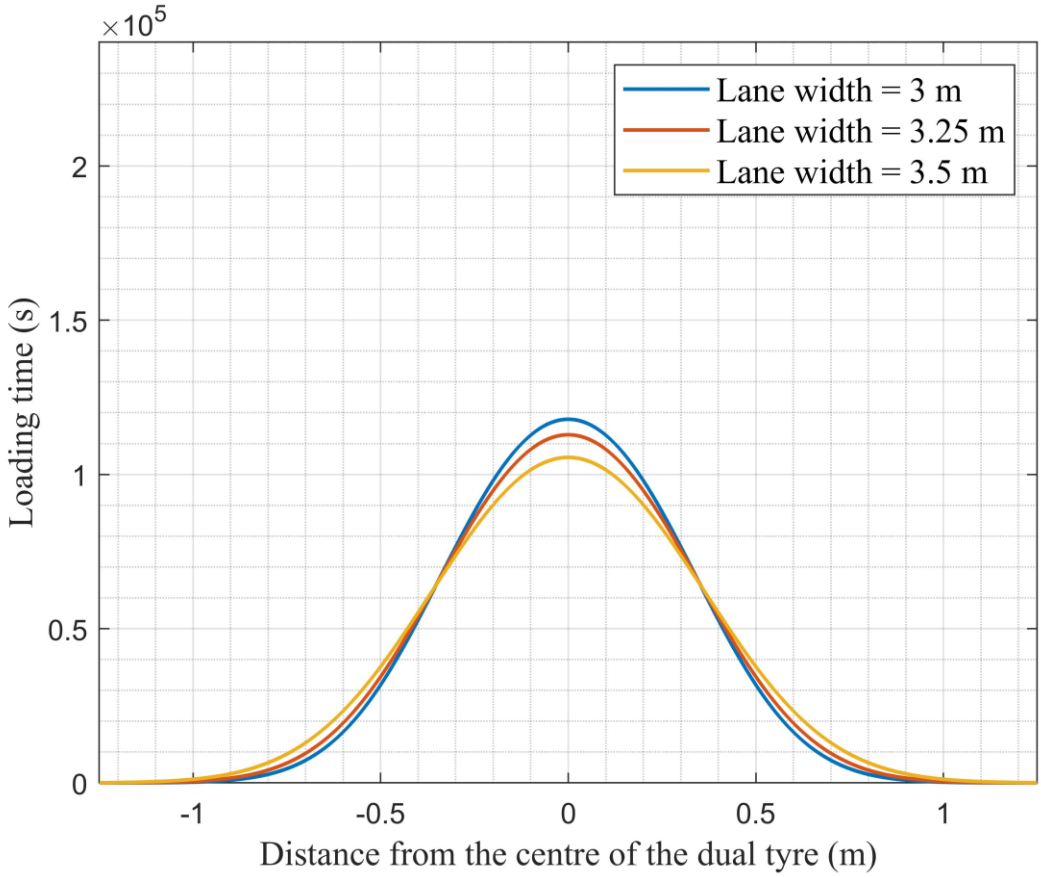

Figure 5 normal distributions of loading time for 100% HDVs for each lane width (reference scenarios)

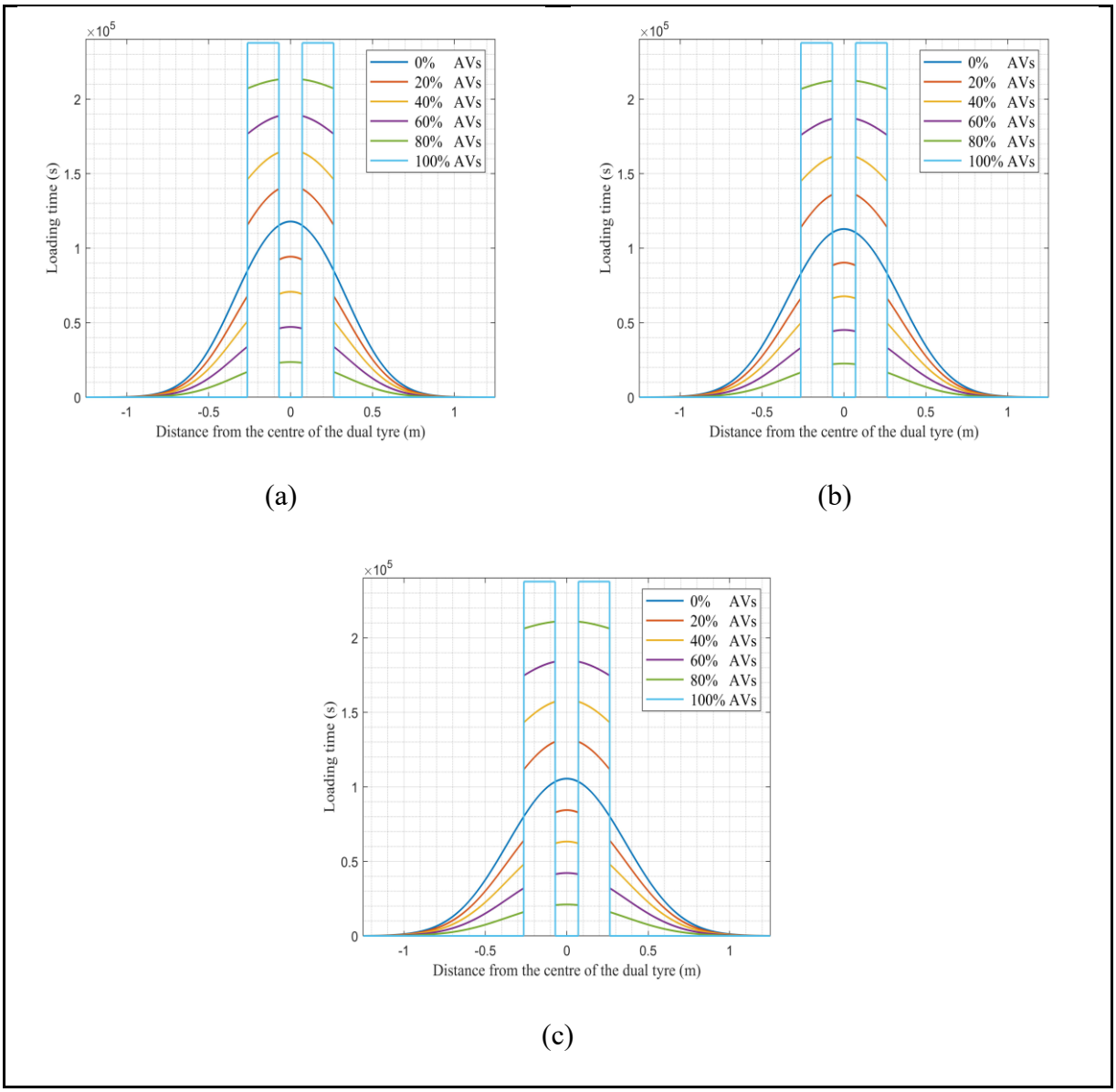

Figure 6 loading time distribution for the mixed traffic of HDVs with normal-wander mode and AVs with zero-wander mode and different penetration rates: a) lane width of 3 m, b) lane width of 3.25 m, c) lane width of 3.5 m

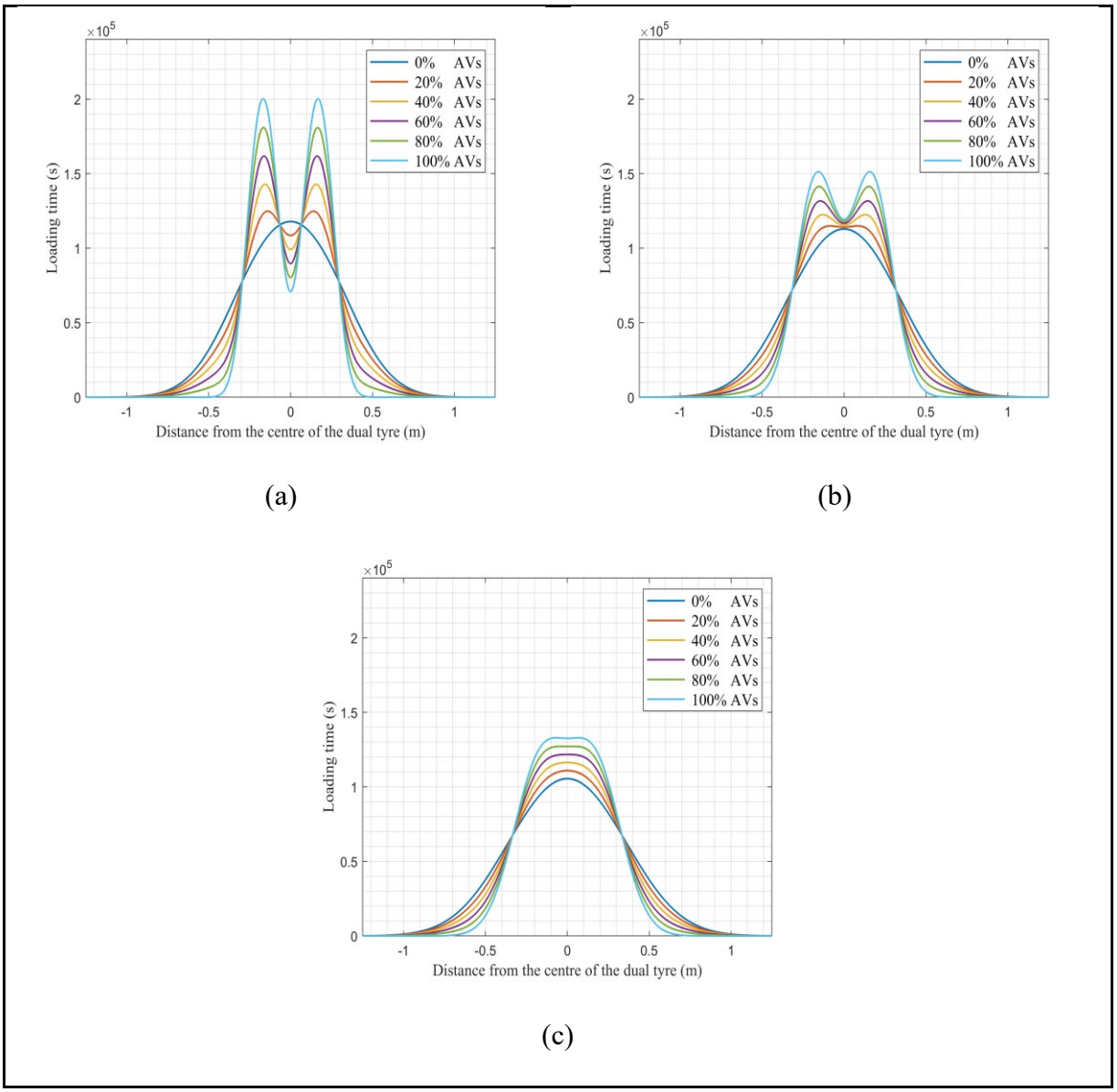

Figure 7 loading time distribution for the mixed traffic of HDVs with normal-wander mode and AVs with normal-wander mode and different penetration rates: a) lane width of 3 m, b) lane width of 3.25 m, c) lane width of 3.5 m

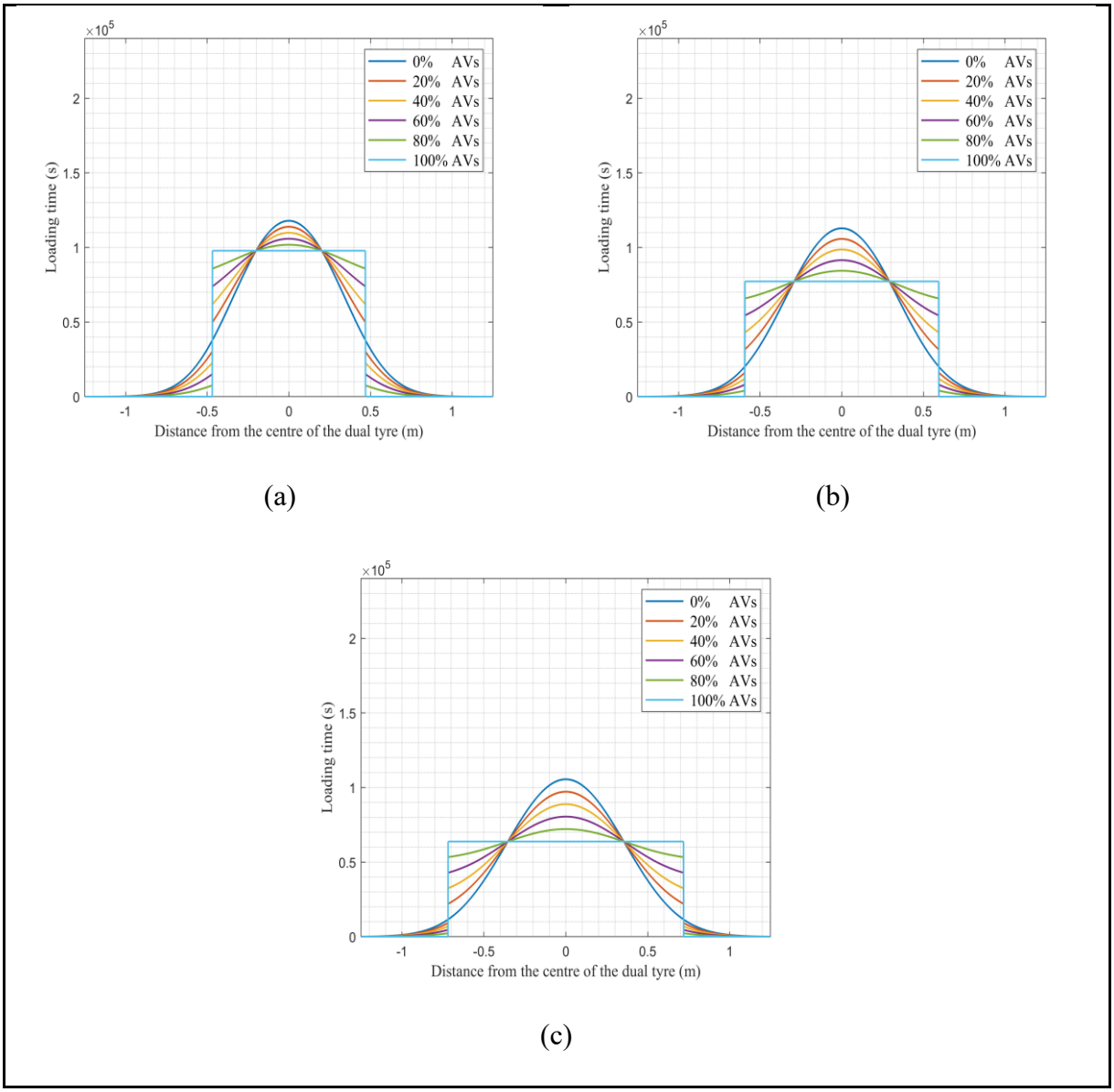

Figure 8 loading time distribution for the mixed traffic of HDVs with normal-wander mode and AVs with uniform-time-wander mode and different penetration rates: a) lane width of 3 m, b) lane width of 3.25 m, c) lane width of 3.5 m

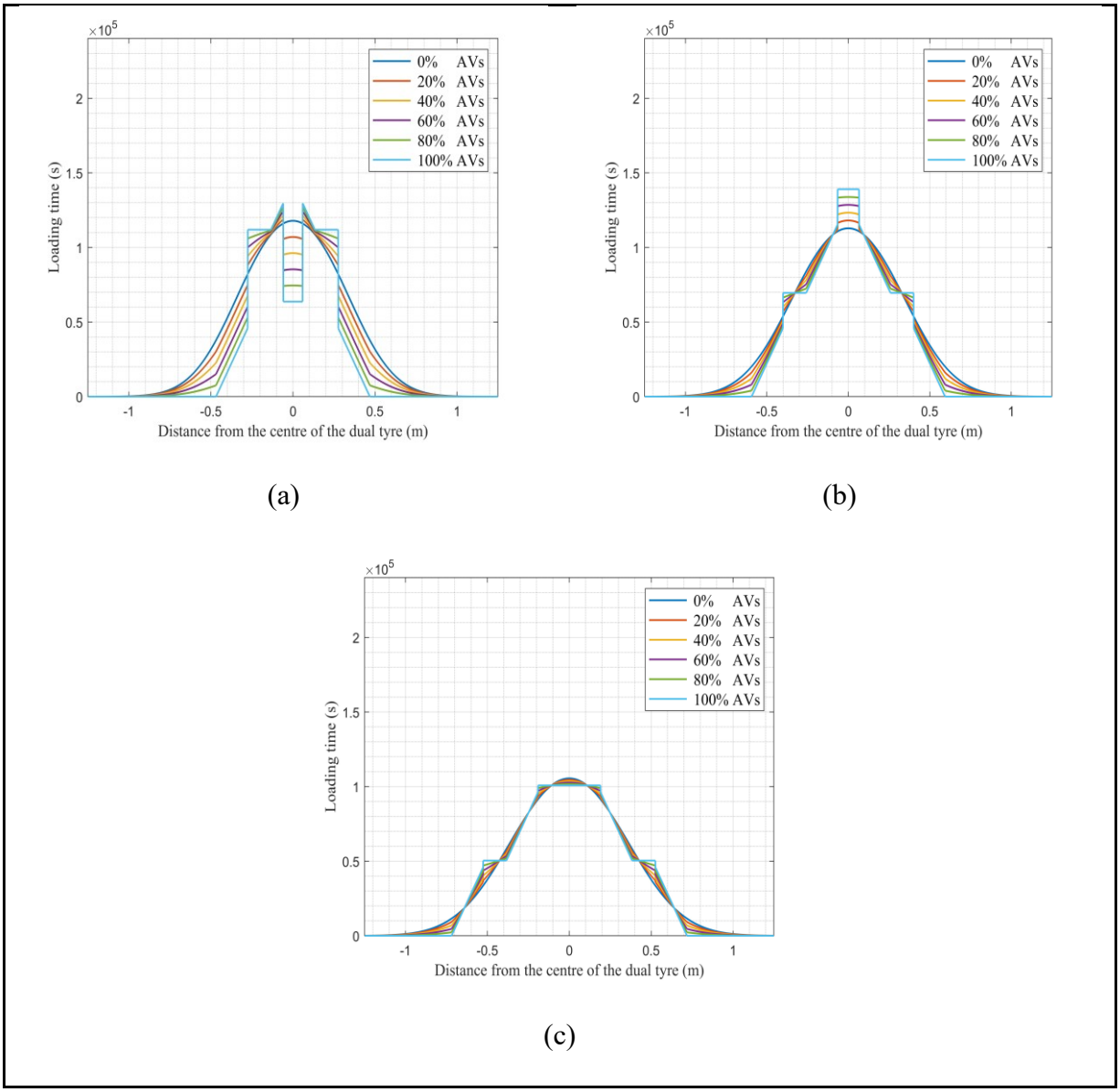

Figure 9 loading time distribution for the mixed traffic of HDVs with normal-wander mode and AVs with uniform-frequency-wander mode and different penetration rates: a) lane width of 3 m, b) lane width of 3.25 m, c) lane width of 3.5 m

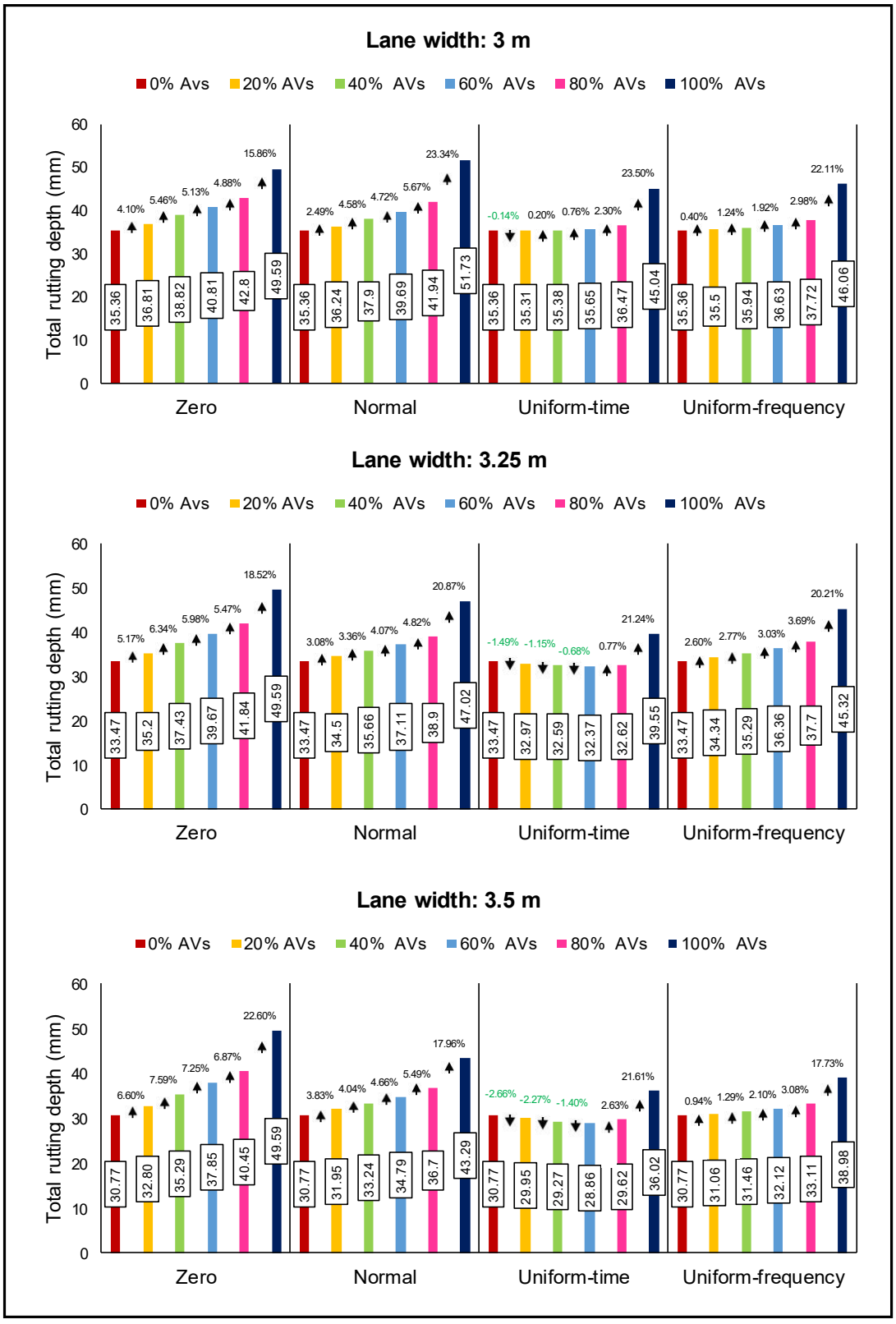

Figure 10 AVs' penetration rate effect on the total rutting depth in all the scenarios

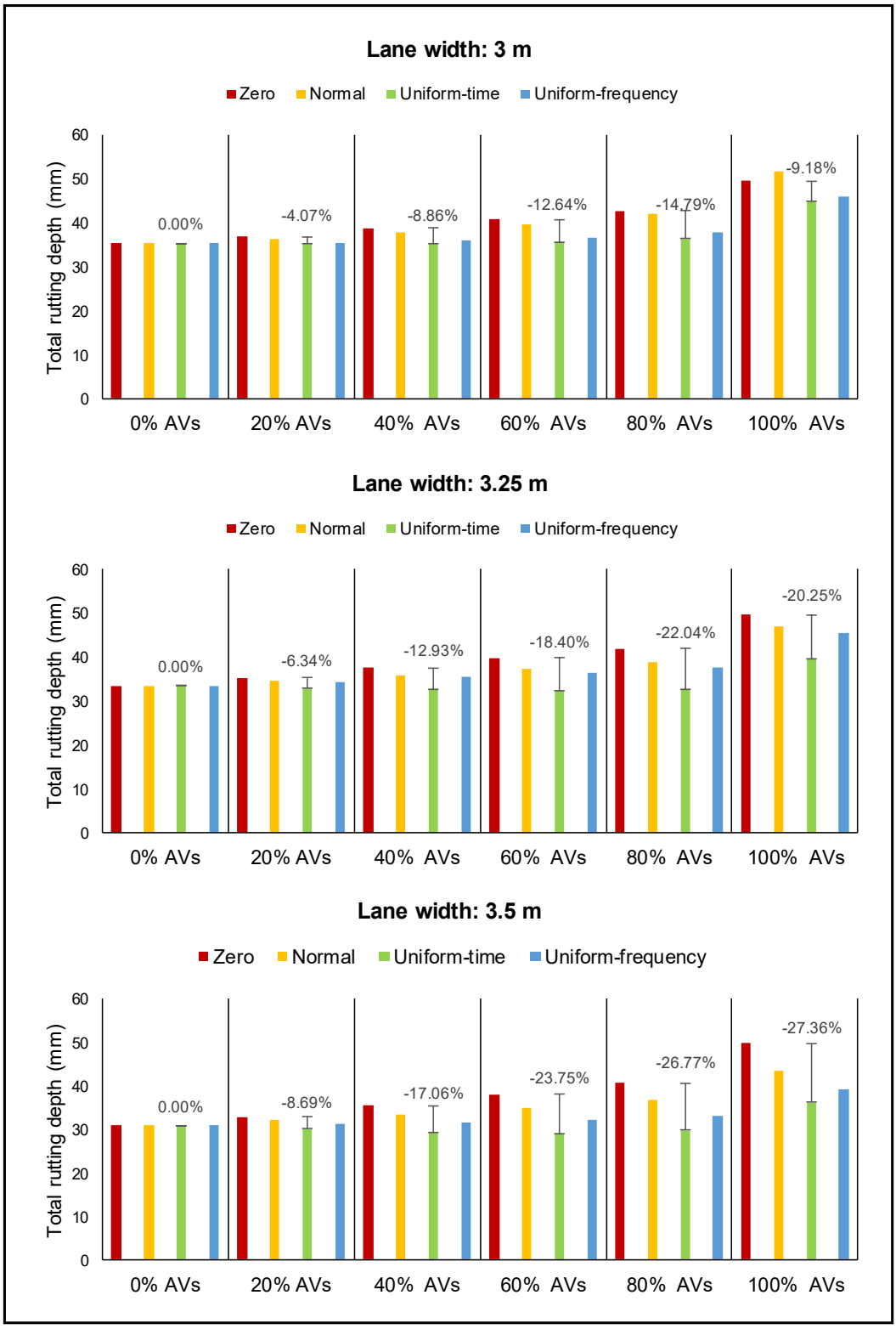

Figure 11 AVs' wander mode effect on total rutting depth in all the scenarios

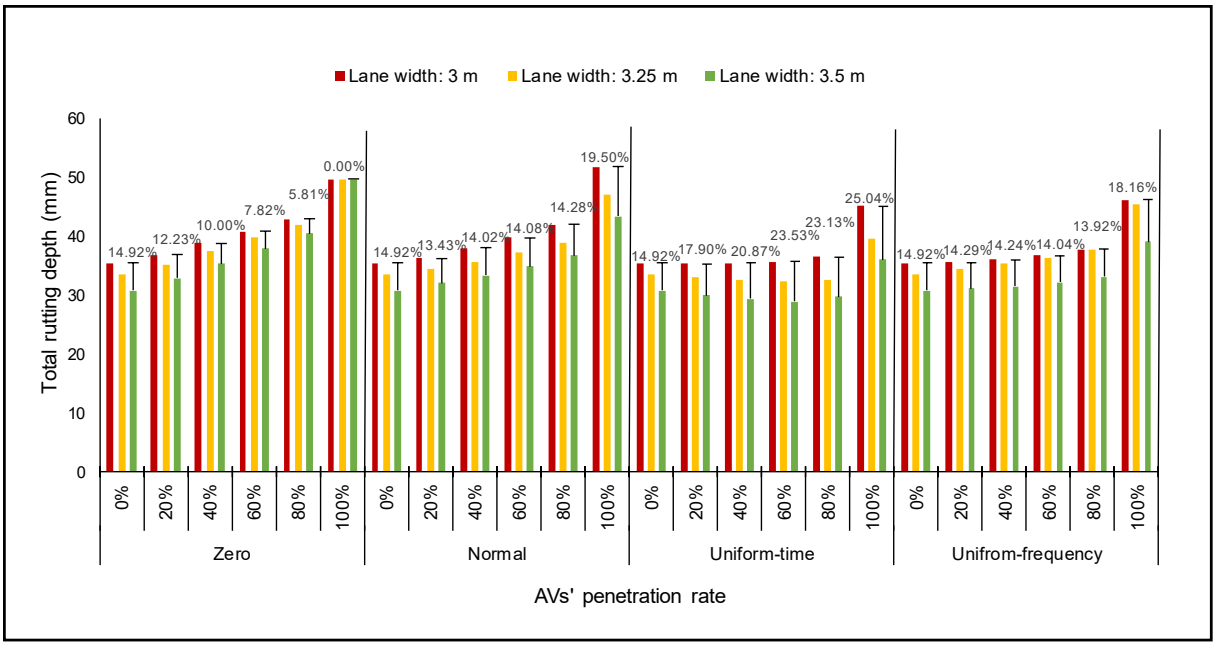

Figure 12 lane width effect on total rutting depth in all the scenarios